Ethanol- and heat-mediated phase change from a kinetic (*Z*' = 4) polymorph to a thermodynamic (*Z*' = 1) polymorph for an N^2,6-diaryl-1,3,5-triazine-2,4-diamine†

Sang Loon Tan,[a] Yee Seng Tan,[a] Muhammad Syafiq Bin Shahari,[b] Ahmad Junaid,[c] Anton V. Dolzhenko[b,d] and Edward R. T. Tiekink[a,*]

[a] Research Centre for Crystalline Materials, School of Medical and Life Sciences, Sunway University, 47500 Bandar Sunway, Selangor Darul Ehsan, Malaysia

[b] School of Pharmacy, Monash University Malaysia, Jalan Lagoon Selatan, Bandar Sunway, Selangor Darul Ehsan 47500, Malaysia

[c] Department of Medicinal Chemistry and Molecular Pharmacology, Purdue University, West Lafayette, Indiana 47907, USA

[d] School of Pharmacy and Biomedical Sciences, Curtin Health Innovation Research Institute, Faculty of Health Sciences, Curtin University, GPO Box U1987, Perth, Western Australia 6845, Australia

***** Electronic Supplementary Materials *****

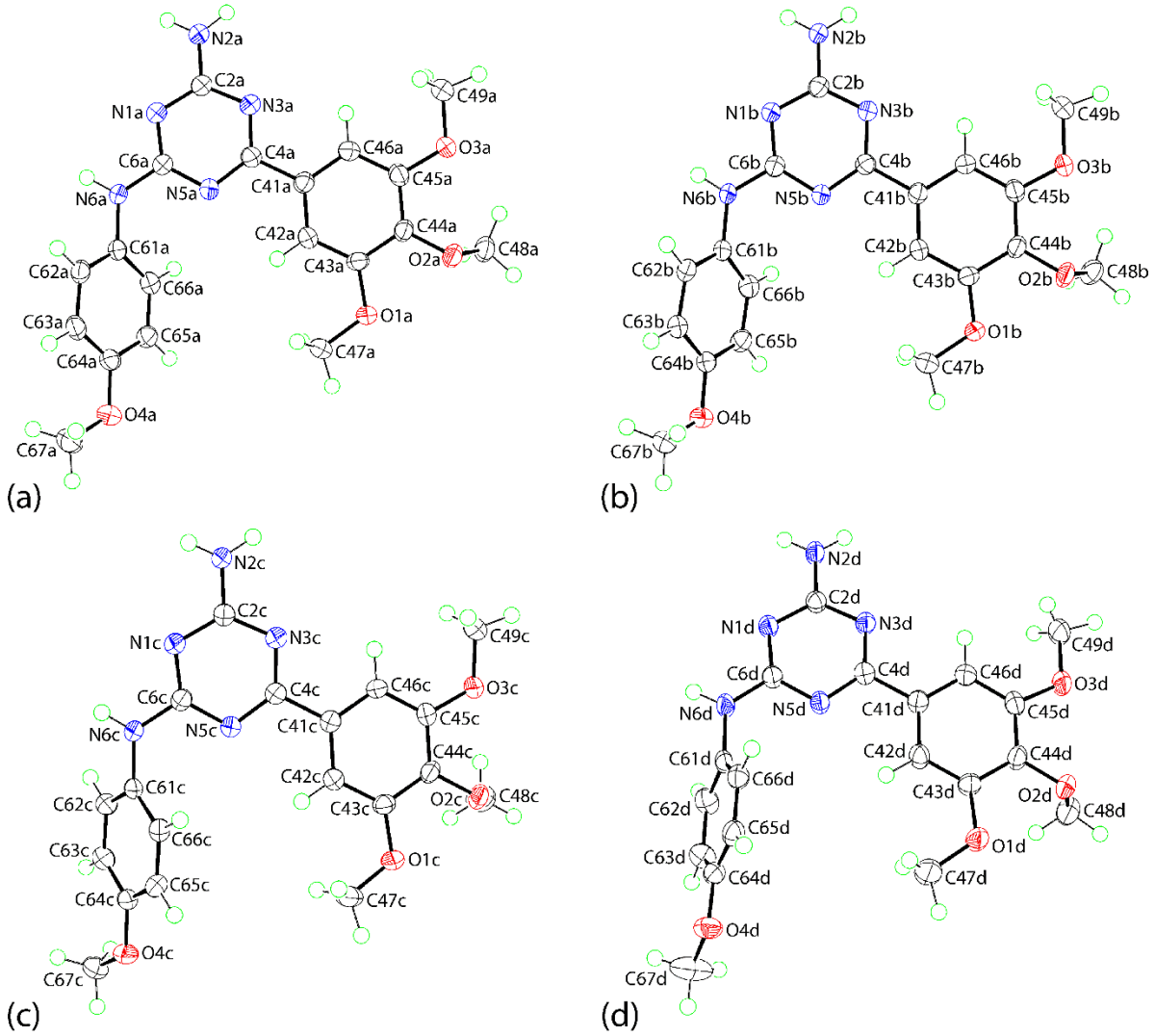

ESI Figure 1. Molecular structures for the four independent molecules comprising the asymmetric unit of the **α**-polymorph: (a) **α**-a, (b) **α**-b, (c) **α**-c and (d) **α**-d, respectively, showing the atom labelling schemes and displacement ellipsoids at the 70% probability level.

ESI Table 1. Selected bond lengths (Å) for polymorph **α**, molecules a–d, polymorph-**β** and the geometry-optimised molecule, **opt-1**

Parameters	**α**-a	**α**-b	**α**-c	**α**-d	**β**	**opt-1**
C2–N1	1.3440(18)	1.3448(17)	1.3489(17)	1.3492(17)	1.3474(12)	1.329
C6–N1	1.3444(18)	1.3452(18)	1.3450(18)	1.3449(18)	1.3472(13)	1.336
C2–N3	1.3485(18)	1.3516(17)	1.3534(17)	1.3525(17)	1.3557(12)	1.340
C4–N3	1.3354(18)	1.3327(17)	1.3327(18)	1.3363(18)	1.3316(13)	1.326
C4–N5	1.3355(18)	1.3368(17)	1.3364(17)	1.3350(17)	1.3347(12)	1.331
C6–N5	1.3448(17)	1.3484(17)	1.3446(17)	1.3498(17)	1.3427(12)	1.329
C2–N2	1.3430(19)	1.3397(18)	1.3377(19)	1.3386(18)	1.3382(13)	1.348
C6–N6	1.3516(18)	1.3539(17)	1.3567(17)	1.3485(17)	1.3538(12)	1.356

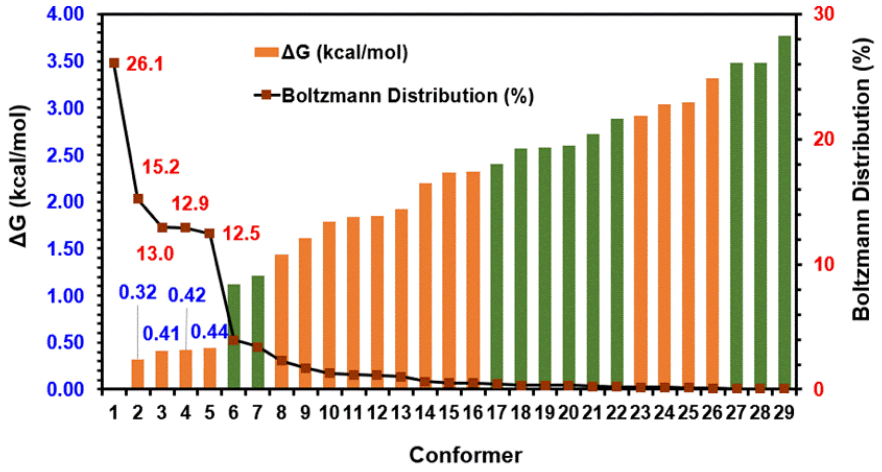

ESI Figure 2. The relative Gibbs free energy and Boltzmann distribution for the identified conformers, **opt-1** to **opt-29**, with the orange bars representing +sp (0 to 30°) or –sp (-30 to 0°) and the green bars representing +ap (150 to 180°) or –ap (-180 to -150°) conformations at σ, respectively. For the purposes of clarity, only the data for the first five conformers are labelled.

Beyond the **opt-5** molecule, marked differences are observed in the relative energies (1.12 to 3.76 kcal/mol) and distributions (0.05 to 3.95%) owing to rotation about σ that leads to +ap (176.7 to 178.5°) and –ap (–178.9 to –176.6°) conformations on top of +sp (2.8 to 4.1°) and –sp (–4.1 to –2.7°) conformations as identified for **opt-1** to **opt-5**.

There is a relaxation of the torsion angles at τ that lead to the formation of additional +sp (17.05 to 18.59°) and –sp (–18.60 to –17.42°) conformations as observed in **opt-7**, **opt-17**, **opt-18**, **opt-20**, **opt-21**, **opt-27** and **opt-28**. On the other hand, the variation in conformation from +sp (1.19 to 1.89°) or –sp (–1.91 to –0.88°) to +ac (107.13 to 110.56°) or –ac (–110.27 to –107.06°) due to the rotation at χ and ω also contributed to a further decrease of stability and distribution as observed for **opt-8** to **opt-29**.

ESI Table 2. Selected torsion angle data (°) for molecules **opt-1** to **opt-29**

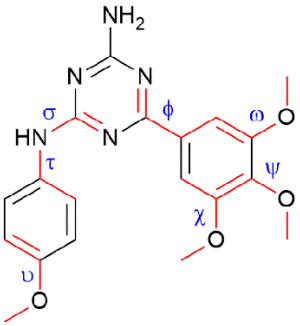

Torsion Angle

	σ	τ	υ	φ	χ	ψ	ω
Opt-1	2.3	–32.9	179.8	–4.6	–1.2	90.6	1.5
Opt-2	2.8	–38.7	–0.2	–3.6	–0.9	–94.8	1.4
Opt-3	–2.7	38.3	–179.4	4.3	–1.4	93.6	1.6
Opt-4	4.1	–43.8	0.2	2.2	1.6	–87.5	–1.6
Opt-5	–4.1	44.0	179.4	2.1	–1.8	87.5	1.6
Opt-6	–178.4	–40.8	179.5	–3.6	–1.3	78.8	1.9
Opt-7	178.5	17.1	–179.6	–0.8	–1.6	89.2	1.5
Opt-8	–3.6	–33.4	0.2	0.1	–1.9	93.3	110.4
Opt-9	–4.1	44.3	–179.4	2.8	–1.3	78.0	110.3
Opt-10	–2.9	39.0	–0.3	4.6	–0.9	79.6	109.8
Opt-11	3.8	–33.0	179.6	0.7	–1.3	79.2	109.8
Opt-12	2.8	–34.5	0.2	–2.6	–107.1	78.0	1.1
Opt-13	4.1	–38.2	–0.2	–2.8	–108.9	102.8	1.2
Opt-14	–3.9	37.9	0.1	2.9	108.6	103.0	–1.1
Opt-15	2.9	–32.9	179.8	–4.8	–109.5	103.0	1.2
Opt-16	–3.0	33.0	–179.9	4.7	109.3	–102.8	–1.2
Opt-17	–178.8	–17.4	179.7	–4.0	–108.0	86.7	1.2
Opt-18	–178.6	17.4	0.1	2.1	107.1	–84.4	1.2
Opt-19	–180.0	38.6	179.8	–0.5	–109.7	101.1	–1.1
Opt-20	178.0	18.6	–179.8	3.7	108.7	–93.4	–1.6
Opt-21	–178.8	–18.6	179.8	–4.8	–109.1	102.2	1.9
Opt-22	178.9	38.6	–179.6	–0.3	107.3	–79.2	–110.3
Opt-23	3.9	–40.0	0.0	–2.1	–107.1	83.6	–108.7
Opt-24	3.8	33.1	–0.2	–0.7	109.6	–102.7	–110.1
Opt-25	–3.9	–34.7	179.5	0.9	110.6	–103.2	110.3
Opt-26	3.6	38.3	–179.4	–0.4	109.8	–93.9	–108.7
Opt-27	–176.9	–17.4	0.1	–0.1	–110.3	79.3	109.4
Opt-28	–178.4	–17.8	179.4	0.2	–110.2	93.2	109.1
Opt-29	–176.6	–32.0	0.3	–0.0	109.2	–86.9	–110.1

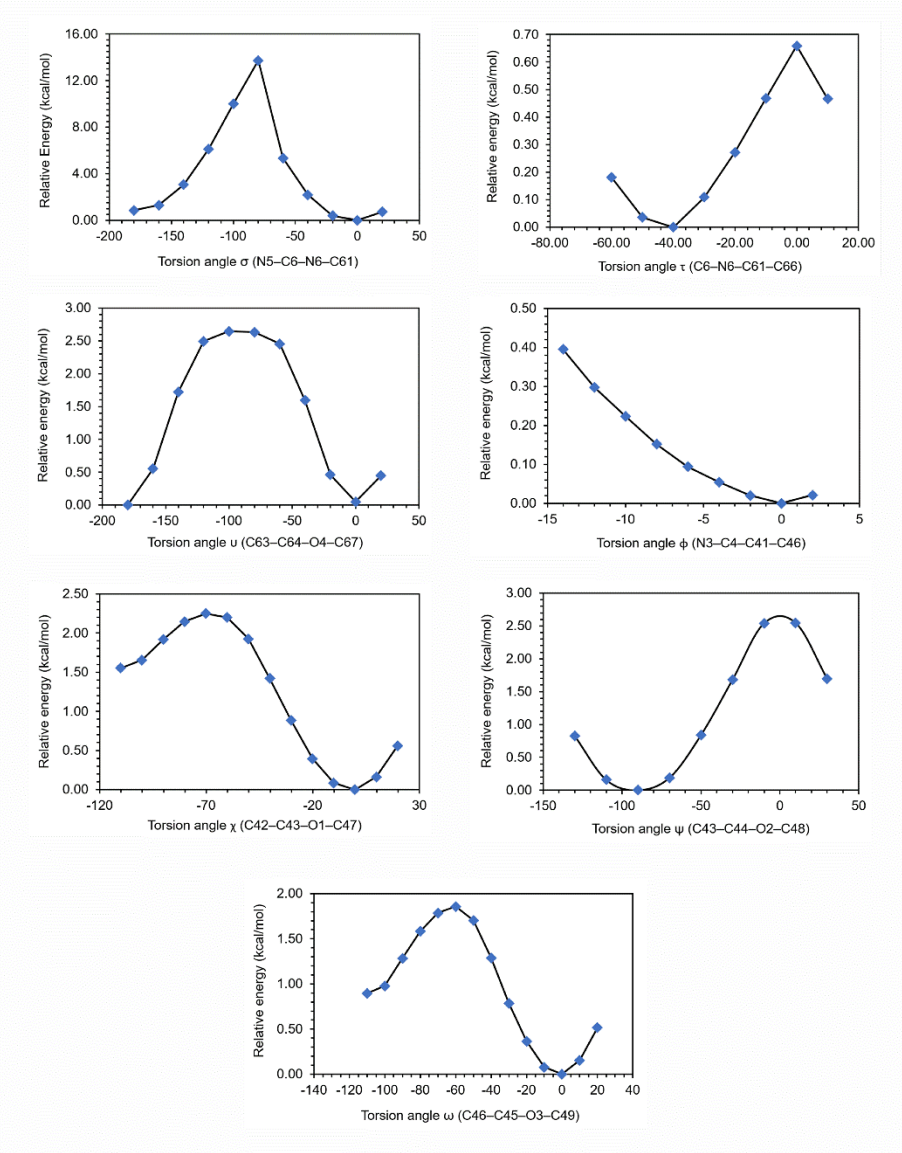

ESI Figure 3. The potential energy profiles upon incremental rotation about the σ, τ, υ, ϕ, χ, ψ and ω, respectively. Owing to the computational cost involved, only rotation around the negative angles were allowed. The simulations show that the potential energies are peaked at approximately –80, –70, –60 and –14° for σ, χ, ω and ϕ, respectively, before gradually stabilising to a minimum at about 0°. Torsion angle υ is most stable at –180° and progressively increases in energy to reach a peak at about –90° before being stabilised again at *ca* 0°. For the ψ and τ torsion angles, the minimum energy is at *ca* –90 and –40°, respectively, with the maximum energy reached at about 0°.

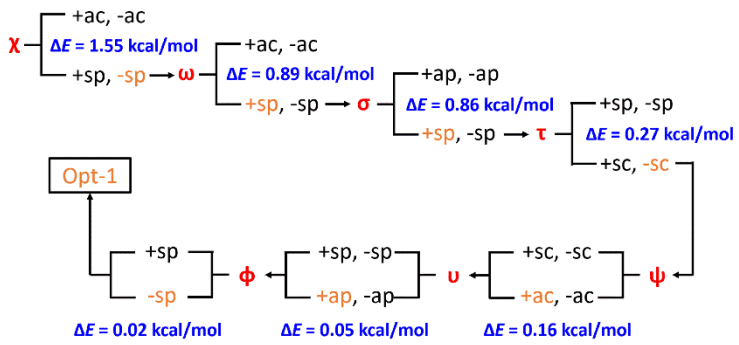

ESI Figure 4. Proposed rank of stability based on the rotational energy barrier at the respective torsion angles.

Opt-22 to **opt-29** are ranked with greatest energy and at the bottom of the Boltzmann distribution mainly because they adopt a +ac or –ac conformation at both χ and ω which have the greatest rotation energy barriers of 1.55 and 0.89 kcal/mol, respectively; to be in the form of +sp or –sp would lead to an improvement in the stability ranking. The rotational energy barrier from +ac/–ac to +sp/–sp for χ is greater than that of ω owing to the steric hindrance from the 4-methoxyphenyl residue. Conformers **opt-12** to **opt-21** have structures with +ac/–ac at χ and +sp/–sp at ω, while the opposite is true for **opt-8** to **opt-11**. The next determining factor in the stability ranking is the rotation at σ which results in two main groups of conformers, *viz*. +ap/–ap and +sp/–sp, of which the former group is relatively less stable with a rotation barrier of about 0.86 kcal/mol. Conformers **opt-6**, **opt-7** as well as other lower ranked structures have +ap/–ap while +sp/–sp is mainly found in **opt-1** to **opt-5**. Moving up the rank of stability is the rotation at τ with an energy barrier of 0.27 kcal/mol from +sp/–sp to +sc/–sc, the former is only observed along with +ap or –ap conformation at σ such as that found in **opt-7** and other lower ranked structures. Rotation about ψ, υ and ϕ positions concludes the ranking in the conformational stability with small energy barriers of 0.16, 0.05 and 0.02 kcal/mol, respectively. This observation leads to interchangeable conformation between +sc/–sc and +ac/–ac for ψ, +sp/–sp and +ap/–ap for υ as well as +sp and –sp for ϕ, all of which occur throughout **opt-1** to **opt-29**.

ESI Table 3. Computed NPA charge (e) for selected atoms in **opt-1**

Atom	**NPA charge**
N1	–0.586
N2	–0.767
H1n	0.402
H2n	0.402
N3	–0.571
N5	–0.580
N6	–0.549
H3n	0.406
C2	0.586
C4	0.469
C6	0.600
C61	0.112
O1	–0.454
O2	–0.475
O3	–0.454
O4	–0.457

ESI Table 4. The hybrid composition of selected natural bonding orbitals for **opt-1**

C···N	C			N		
	Overall occupancy (%)	*s* (%)	*p* (%)	Overall occupancy (%)	*s* (%)	*p* (%)
C2–N2	59.5	31.1	68.9	40.5	37.8	61.9
C6–N6	60.5	30.8	69.2	39.5	36.3	63.4
C61–N6	60.9	28.2	71.8	39.1	36.6	63.2

ESI Table 5. A summary of the geometric parameters (Å, º) characterising the identified intermolecular contacts in the crystals of the **α**- and **β**-polymorphs

Contact	H···B	A···B	A–H···B	Symmetry operation
α				
Intra-layer region				
N6a–H3n···N1d	2.216(16)	3.1074(16)	169.4(14)	$2 - x, -\frac{1}{2} + y, \frac{3}{2} - z$
N2a–H2n···O1c	2.246(16)	3.1443(16)	175.6(14)	$x, \frac{1}{2} - y, -\frac{1}{2} + z$
N6b–H6n···N1c	2.237(16)	3.0963(16)	167.5(14)	x, y, z
N2b–H5n···O1d	2.269(16)	3.1511(17)	177.2(14)	$1 - x, 1 - y, 1 - z$
N6c–H9n···N1b	2.301(16)	3.1693(16)	171.3(15)	x, y, z
N2c–H8n···O1a	2.341(17)	3.2219(16)	173.5(16)	$x, \frac{3}{2} - y, \frac{1}{2} + z$
N6d–H12n···N1a	2.127(16)	3.0425(16)	168.6(14)	$2 - x, \frac{1}{2} + y, \frac{3}{2} - z$
N2d–H11n···O1b	2.244(16)	3.1026(16)	166.9(14)	$1 - x, 2 - y, 1 - z$
C67b–H67f···O3a	2.55	3.3175(17)	135	$x, \frac{3}{2} - y, \frac{1}{2} + z$
C49a–H49b···O4c	2.49	3.3368(18)	145	$x, \frac{1}{2} - y, -\frac{1}{2} + z$

C49d–H49k···O4b	2.53	3.477(2)	161	$1-x, 2-y, 1-z$
C67c–H67h···O4b	2.59	3.4514(17)	147	$x, -1+y, z$
C49c–H49h···O4a	2.56	3.3931(19)	143	$x, \frac{3}{2}-y, \frac{1}{2}+z$
C49b–H49e···O4d	2.34	3.2901(19)	164	$1-x, 1-y, 1-z$
C67a–H67b···O4d	2.57	3.4580(19)	151	$2-x, \frac{1}{2}+y, \frac{3}{2}-z$
Inter-layer region				
C47c–H47g···O1a	2.51	3.4361(18)	158	$1-x, 1-y, 1-z$
C63a–H63a···O2d	2.56	3.4396(16)	154	x, y, z
C63b–H63b···O2c	2.39	3.3216(16)	165	$1-x, \frac{1}{2}+y, \frac{3}{2}-z$
C48d–H48j···N3a	2.56	3.4490(19)	151	$x, \frac{1}{2}-y, \frac{1}{2}+z$
C62b–H62b···N2a	2.50	3.3381(19)	147	$1-x, 1-y, 1-z$
Cg(N1b,N3b,N5b,C2b,C4b,C5b)···				
Cg(N1d,N3d,N5d,C2d,C4d,C5d)	–	3.7690(7)	3.42(6)[a]	$-1+x, \frac{3}{2}-y, -\frac{1}{2}+z$
C63d–H63d··· Cg(N1d,N3d,N5d,C2d,C4d,C5d)	2.70	3.5702(16)	153	$2-x, 1-y, 2-z$

β

N6–H3n···N1	2.144(10)	3.0196(12)	173.1(11)	$-x, 1-y, 1-z$
N2–H2n···O1	2.085(11)	2.9543(12)	171.8(11)	$\frac{3}{2}-x, \frac{1}{2}+y, \frac{3}{2}-z$
Cg(N1,N3,N5,C2,C4,C5)···Cg(N1,N3,N5,C2,C4,C5)	–	3.4964(5)	0[a]	$1-x, 1-y, 1-z$
C62–H62···Cg(C41-C46)	2.85	3.6450(11)	141	$-1+x, y, z$
C67–H67a···Cg(C41-C46)	2.86	3.7698(15)	155	$-\frac{1}{2}+x, \frac{1}{2}-y, -\frac{1}{2}+z$
C48–H48b···Cg(C61-C66)	2.93	3.8184(12)	152	$\frac{3}{2}+x, \frac{1}{2}-y, \frac{1}{2}+z$

a value refers to the angle between the specified aromatic rings

ESI Table 6. The d_{norm} contact distances (adjusted to neutron values) for all identified interactions present in the individual molecules of the **α**- and **β**-polymorphs with respect to the corresponding sum of van der Waals radii

Contact (Donor···Acceptor)	Distance (Å)	ΣvdW (Å)	Symmetry operation
α-a			
N6a–H3n···N1d	2.11	2.64	$2-x, -\frac{1}{2}+y, \frac{3}{2}-z$
N2a–H2n···O1c	2.14	2.61	$x, \frac{1}{2}-y, -\frac{1}{2}+z$
C49a–H49b···O4c	2.41	2.61	$x, \frac{1}{2}-y, -\frac{1}{2}+z$
N2a–H2n···O2c	2.57	2.61	$x, \frac{1}{2}-y, -\frac{1}{2}+z$
N2a–H1n···C62d	2.78	2.79	$2-x, -\frac{1}{2}+y, \frac{3}{2}-z$
C63a–H63a···O2d	2.44	2.61	x, y, z
C67a–H67b···O4d	2.48	2.61	$2-x, \frac{1}{2}+y, \frac{3}{2}-z$
C62a–H62a···N2b	2.53	2.64	$1-x, 1-y, 1-z$
C67a–H67a···O3d	2.57	2.61	x, y, z
C67a–H67c···O3b	2.57	2.61	$1+x, \frac{3}{2}-y, \frac{1}{2}+z$
C48a–H48a···N1b	2.58	2.64	$1-x, -\frac{1}{2}+y, \frac{1}{2}-z$
α-b			
N6b–H6n···N1c	2.11	2.64	x, y, z
N2b–H5n···O1d	2.14	2.61	$1-x, 1-y, 1-z$
C49b–H49e···O4d	2.24	2.61	$1-x, 1-y, 1-z$
N2b–H5n···O2d	2.57	2.61	$1-x, 1-y, 1-z$
N2b–H4n···C62c	2.66	2.79	x, y, z
C63b–H63b···O2c	2.27	2.61	$1-x, \frac{1}{2}+y, \frac{3}{2}-z$
C67b–H67f···O3a	2.48	2.61	$x, \frac{3}{2}-y, \frac{1}{2}+z$

C48b–H48e···C63a	2.78	2.79	$-1+x, \frac{3}{2}-y, -\frac{1}{2}+z$
α-c			
N6c–H9n···N1b	2.17	2.64	x, y, z
N2c–H8n···O1a	2.22	2.61	$x, \frac{3}{2}-y, \frac{1}{2}+z$
C49c–H49h···O4a	2.48	2.61	$x, \frac{3}{2}-y, \frac{1}{2}+z$
N2c–H8n···O2a	2.56	2.61	$x, \frac{3}{2}-y, \frac{1}{2}+z$
N2c–H7n···C62b	2.36	2.79	x, y, z
C47c–H47g···O1a	2.42	2.61	$1-x, 1-y, 1-z$
C67c–H67h···O4b	2.50	2.61	$x, -1+y, z$
C48c–H48g···C45d	2.55	2.79	x, y, z
C48c–H48h···C63d	2.56	2.79	$2-x, 1-y, 2-z$
C48c–H48g···C46d	2.63	2.79	x, y, z
C47c–H47g···C43a	2.76	2.79	$1-x, 1-y, 1-z$
α-d			
N6d–H12n···N1a	2.05	2.64	$2-x, \frac{1}{2}+y, \frac{3}{2}-z$
N2d–H11n···O1b	2.11	2.61	$1-x, 2-y, 1-z$
C49d–H49k···O4b	2.44	2.61	$1-x, 2-y, 1-z$
N2d–H11n···O2b	2.60	2.61	$1-x, 2-y, 1-z$
N2d–H10n···C62a	2.45	2.79	$2-x, \frac{1}{2}+y, \frac{3}{2}-z$
C48d–H48j···N3a	2.47	2.64	$x, \frac{1}{2}-y, \frac{1}{2}+z$
β			
N6–H3n···N1	2.02	2.64	$-x, 1-y, 1-z$

N2–H2n···O1	1.95	2.61	$^{3}/_{2} - x, \frac{1}{2} + y, {}^{3}/_{2} - z$
N2–H2n···O2	2.49	2.61	$^{3}/_{2} - x, \frac{1}{2} + y, {}^{3}/_{2} - z$
N2–H1n···C62	2.34	2.79	$-x, 1 - y, 1 - z$
C62–H62···C43	2.61	2.79	$-1 + x, y, z$
C47–H47c···N3	2.58	2.64	$^{3}/_{2} - x, \frac{1}{2} + y, {}^{3}/_{2} - z$
C66–H66···N2	2.63	2.64	$1 - x, 1 - y, 1 - z$
H46···H47c	2.10	2.18	$^{3}/_{2} - x, \frac{1}{2} + y, {}^{3}/_{2} - z$

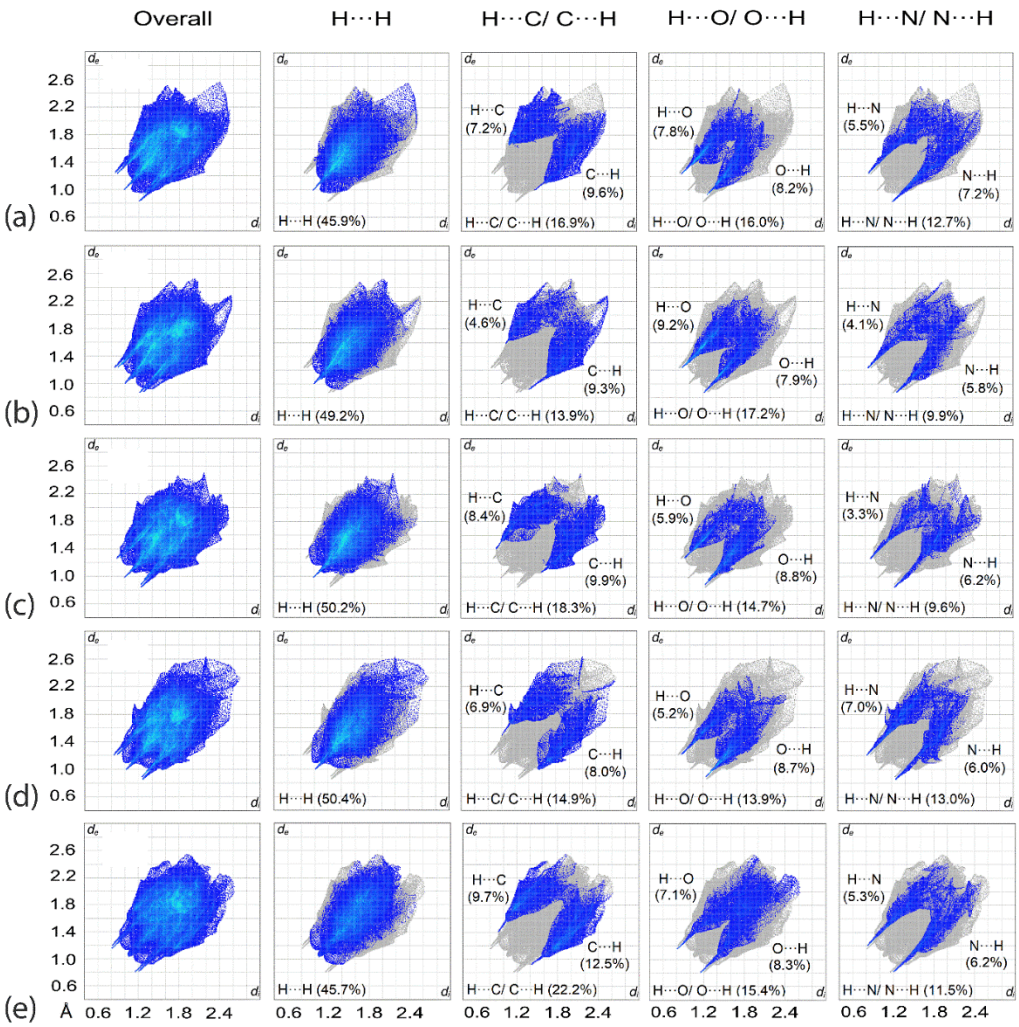

ESI Figure 5. The overall two-dimensional fingerprint and decomposed plots delineated into specific contacts along with the distribution for (a) **α**-a, (b) **α**-b, (c) **α**-c, (d) **α**-d and (e) **β**.

ESI Table 7. Interaction energies (kcal/mol) for the weaker close contacts present in the crystal of the **α**-polymorph of **1**

Close contact	E_{ele}	E_{pol}	E_{disp}	E_{rep}	E_{int}	Symmetry operation
C48c–H48g···C45d + C48c–H48g···C46d	–3.0	–0.3	–9.2	5.8	–6.6	x, y, z
C67c–H67h···O4b	–3.7	–0.9	–4.2	2.7	–6.0	$x, -1+y, z$
C63a–H63a···O2d + C67a–H67a···O3d	–3.2	–0.8	–4.5	2.8	–5.6	x, y, z
C48d–H48j···N3a	–1.1	–0.4	–6.7	2.6	–5.6	$x, \frac{1}{2}-y, -\frac{1}{2}+z$
C67b–H67f···O3a	–2.6	–0.5	–5.0	3.1	–5.0	$x, \frac{3}{2}-y, -\frac{1}{2}+z$
C67a–H67c···O3b + C48b–H48e···C63a	–2.3	–0.4	–4.6	2.6	–4.8	$1+x, \frac{3}{2}-y, \frac{1}{2}+z$
C62a–H62a···N2b + C62b–H62b···N2a	–2.3	–0.3	–5.3	4.1	–3.8	$1-x, 1-y, 1-z$
C67a–H67b···O4d	–2.0	–0.2	–1.9	1.2	–2.9	$2-x, \frac{1}{2}+y, \frac{3}{2}-z$
C63b–H63b···O2c	–2.0	–0.2	–1.9	1.2	–2.9	$1-x, \frac{1}{2}+y, \frac{3}{2}-z$
C48d–H48k···C63c	–0.6	–0.3	–3.7	2.2	–2.5	$1-x, 1-y, 1-z$
C48c–H48h···C63d	–0.7	–0.3	–3.6	2.6	–2.0	$2-x, 1-y, 2-z$
C48b–H48f···C48b	–0.5	0.0	–2.1	1.0	–1.5	$-x, 2-y, -z$

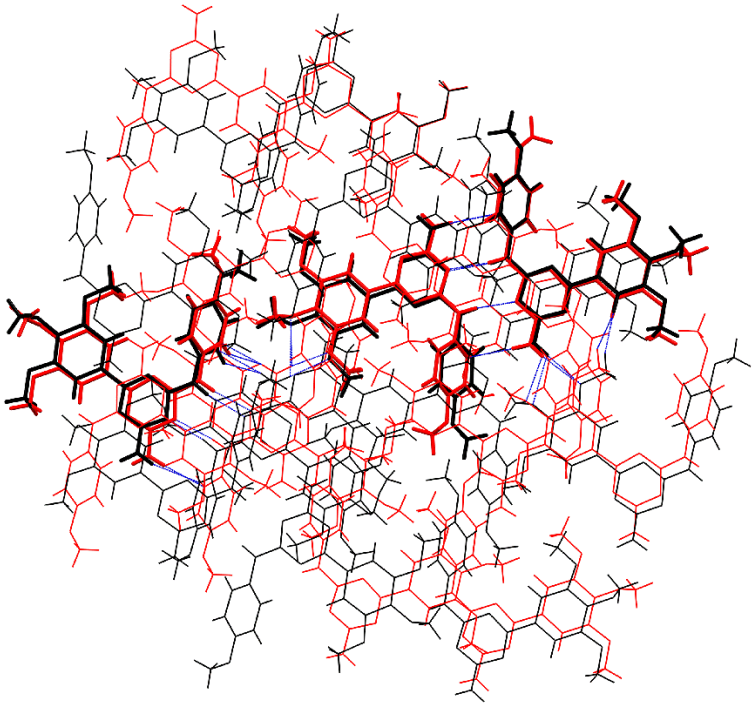

ESI Figure 6. The molecular packing analysis between the **α**- (black) and **β**- (red) polymorphs, showing three (in capped stick representation) out of 15 molecules (in wireframe) overlapped. The overlapped molecules in both polymorphs exhibit common interaction patterns as illustrated by the blue dotted line.

ESI Table 8. Unit-cell data on a single crystal for a heating/cooling cycle showing the irreversible SCSC phase change from the **α**- to **β**-polymorph. The unit-cell data for the first measurement at 298 K corresponds to the **α**-polymorph, whereas the unit-cell data for the subsequent experiments, *i.e.* 398, 298 and 100 K, correspond to the **β**-polymorph

First unit-cell determination (298 K):

_cell_length_a	19.0392(18)
_cell_length_b	18.0969(14)
_cell_length_c	22.660(2)
_cell_angle_alpha	90.0
_cell_angle_beta	104.539(9)
_cell_angle_gamma	90.0
_cell_volume	7558(1)
_cell_measurement_temperature	297.95(10)

Second unit-cell determination (398 K):

_cell_length_a	8.181(5)
_cell_length_b	17.597(7)
_cell_length_c	15.685(7)
_cell_angle_alpha	90.0
_cell_angle_beta	103.16(5)
_cell_angle_gamma	90.0
_cell_volume	2199(2)
_cell_measurement_temperature	397.98(10)

Third unit-cell determination (298 K):

_cell_length_a	8.229(5)
_cell_length_b	17.654(9)
_cell_length_c	15.378(9)
_cell_angle_alpha	90.0
_cell_angle_beta	102.50(6)
_cell_angle_gamma	90.0
_cell_volume	2181(2)
_cell_measurement_temperature	297.99(10)

Fourth unit-cell determination (100 K):

_cell_length_a	8.070(5)
_cell_length_b	17.291(18)
_cell_length_c	14.256(7)
_cell_angle_alpha	90.0
_cell_angle_beta	101.48(6)
_cell_angle_gamma	90.0
_cell_volume	1949(3)
_cell_measurement_temperature	99.98(10)

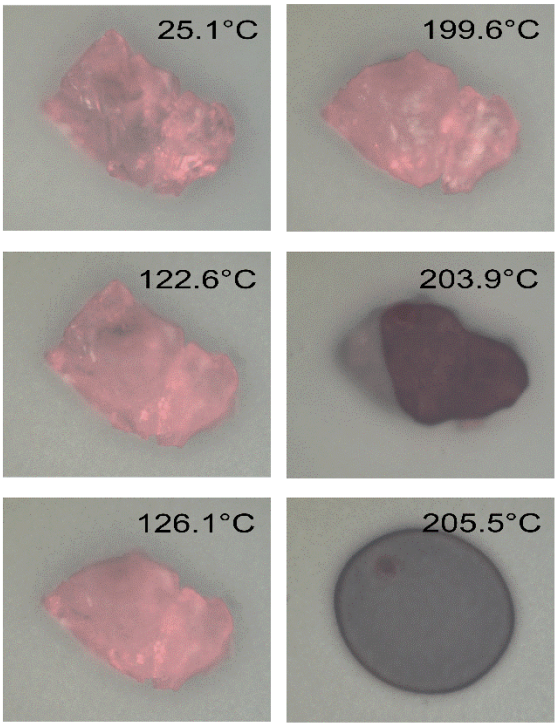

(a)

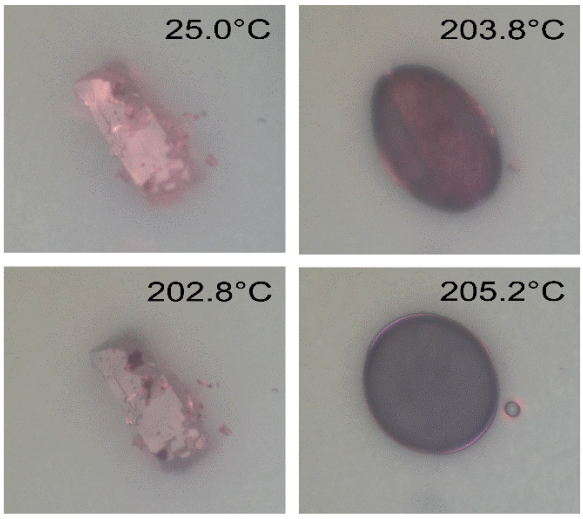

(b)

ESI Figure 7. Images of the heating cycle in the thermo-microscopic study for the (a) **α**-polymorph and (b) **β**-polymorph. The key result is the same melting events between 203–206 °C.